PUBLICATIONS OF THE ASTRONOMICAL SOCIETY OF THE PACIFIC, **114**:284–297, 2002 March
© 2002. The Astronomical Society of the Pacific. All rights reserved. Printed in U.S.A.

Selection of High-*z* Supernova Candidates

TOMAS DAHLÉN

Stockholm Observatory, Stockholm Centre for Physics, Astronomy and Biotechnology, SE-106 91 Stockholm, Sweden; tomas@astro.su.se

AND

ARIEL GOOBAR

Physics Department, Stockholm University, Stockholm Centre for Physics, Astronomy and Biotechnology, SE-106 91 Stockholm, Sweden; ariel@physto.se

Received 2001 October 23; accepted 2001 December 21; published 2002 February 6

ABSTRACT. Deep, ground-based, optical wide-field supernova searches are capable of detecting a large number of supernovae over a broad redshift range up to $z \sim 1.5$. While it is practically infeasible to obtain spectroscopic redshifts of all supernova candidates right after their discovery, we show that the magnitudes and colors of the host galaxies, as well as the supernovae, can be used to select high-*z* supernova candidates for subsequent spectroscopic and photometric follow-up.

Using Monte Carlo simulations we construct criteria for selecting galaxies in well-defined redshift bands. For example, with a selection criterion using $B-R$ and $R-I$ colors we are able to pick out potential host galaxies for which $z \geq 0.85$ with an 80% confidence level and with a selection efficiency of 64%–86%. The method was successfully tested using real observations from the Hubble Deep Field.

Similarly, we show that the magnitude and colors of the supernova discovery data can be used to constrain the redshift. With a set of cuts based on $V-R$ and $R-I$ in a search to $m_I \sim 25$, supernovae at $z \sim 1$ can be selected in a redshift interval $\sigma_z \leq 0.15$.

1. INTRODUCTION

High-*z* Type Ia supernovae (SNe) have been shown to be very accurate tools for studying cosmological parameters (Perlmutter et al. 1999; Riess et al. 1998). As the sensitivity of the magnitude-redshift relation increases with the size of the redshift range probed, searches for SNe at redshifts $z \gtrsim 1$ become crucial to refining our understanding of cosmology (Goobar & Perlmutter 1995; Goliath et al. 2001).

One of the difficulties in searches dedicated to high-*z* SNe is the selection of candidates for subsequent follow-up. An *I*-band SN search down to $m_I \sim 25$ generates candidates in a broad redshift range: $0.1 < z \lesssim 1.5$. On a 1 deg^2 detection image, separated by 3 weeks from a reference image, there will be about a dozen Type Ia SNe on the rising part of the light curve.

Additional information is required to make the follow-up of $z > 0.85$ SNe efficient. This is particularly important because the follow-up of candidates with space instruments, such as the *Hubble Space Telescope*, needs to be decided on very soon after discovery, leaving limited time for prior spectroscopic screening.

In this paper we discuss how broadband photometry of the host galaxy, as well as the SN, can be used in order to select targets with $\sigma_z \sim 0.15$ with high efficiency. We focus on the optical bands, producing mainly SNe up to $z \sim 1.5$. In § 2 we discuss the SN rates that are used in our simulations. In § 3 we study the use of host galaxy magnitudes and colors to estimate the redshift of an SN candidate, followed by a discussion in § 4 on how deep a survey must be in order to obtain the required galaxy colors. In § 5 we discuss the use of SN magnitude and color for redshift estimation. Finally, a summary and conclusions are given in § 6.

In this paper we assume a flat cosmology with $\Omega_M = 0.3$ and $\Omega_\Lambda = 0.7$ and a Hubble constant $H_0 = 65$ km s^{-1} Mpc^{-1}. Magnitudes are given in the standard Vega-based system.

2. SN RATES

Models of high-*z* SN rates predict an increase out to $z \sim 1.5$ (Madau, Della Valle, & Panagia 1998; Dahlén & Fransson 1999). This increase reflects the observed increase in the star formation in galaxies out to these redshifts (e.g., Madau, Pozzetti, & Dickinson 1998). At higher redshifts the evolution of the star formation rate, and therefore the SN rate, is more uncertain. This is mainly due to the uncertainty in the amount of dust extinction affecting observations of high-*z* galaxies. A direct relation between star formation rate and SN rate is, however, valid only for core-collapse SNe (Types II and Ib/c), where the SN progenitor is a short-lived star. For Type Ia SNe there is an unknown time delay between the formation of the SN progenitor star and the explosion of the SN. In the models cited above, a parameter τ is introduced to represent this time delay. Considered values of τ lie in the range 0.3–3 Gyr.

Calculating the absolute numbers for the SN rates involves a number of parameters, such as the distribution of SN types, peak luminosities, light curves, initial mass function, cosmology, and, most important, assumptions about dust extinction. Estimated rates could therefore have an uncertainty of about a factor of 2–3. Using simulations described in Dahlén & Fransson (1999), we estimate that a detection image, taken 3 weeks after a reference image, should result in ~20–45 SNe per deg^2. Here we have used a limiting magnitude $m_I = 25$ and a detection criterion where the SNe on the second image are more than 0.5 mag brighter than on the reference image. Approximately one-half of the SNe are Type Ia that are still brightening.

In this paper we are not directly affected by the absolute value of the SN rate at different z, since the aim here is to estimate the redshift for SN candidates already detected. However, in our simulations we estimate the redshift *distribution* of the observable SNe; therefore, the relative evolution of the SN rate with z must be considered. In our models we use both a constant and an evolving Type Ia SN rate, where the latter is taken from the theoretical models in Dahlén & Fransson (1999).

Figure 1 shows the differential observable Type Ia SN rate versus redshift (arbitrary units) for models with constant SN rate (*solid line*) and evolving rates with $\tau = 1.0$ Gyr (*dashed line*) and $\tau = 3.0$ Gyr (*dotted line*). The distribution was generated with a Monte Carlo (MC) simulation of 10^5 SNe (for each model) up to a redshift $z = 2$. The integrated rate is normalized to unity for all three cases.

Note that the shape of the distribution is given by two effects as one moves from intrinsic rates to rates in the observer's frame: the volume effect makes the number of high-z SNe increase to $z \sim 1.8$, and the cosmological time dilation makes the rates fall as $(1 + z)^{-1}$.

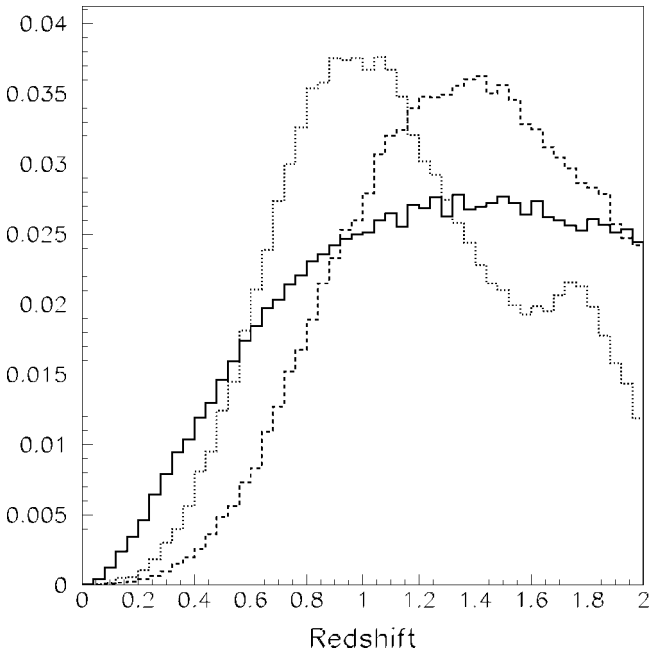

FIG. 1.—Differential observable Type Ia SN rate as a function of redshift for three models (arbitrary units), where the integrated rate up to $z = 2$ has been normalized to 1 using 10^5 MC simulated SNe. The solid line assumes a constant SN rate per comoving volume. The dashed line shows the observable rate for $\tau = 1$ Gyr, the dotted line $\tau = 3$ Gyr. Note that apart from the volume effect, the observable rate falls as $(1 + z)^{-1}$ because of the cosmological time dilation.

3. SELECTION BY HOST GALAXY COLORS

Using the magnitude and colors of the host galaxy to select SN candidates has the advantage that a catalog listing probable high-z galaxies can be constructed in advance. When an SN is detected, it is possible to immediately determine whether it is a high-z candidate. In addition, the host galaxy redshift gives an estimate of the absolute magnitude of the SN, which can set constraints regarding SN type, since SNe Ia have brighter peak luminosities than other SN types, except for a small fraction of extremely luminous core-collapse SNe. This is important since an increasing fraction of the SNe will be Type Ib/c or II as one reaches for fainter magnitude limits.

Using host galaxy magnitudes requires deep images of the survey field from which colors can be obtained. The limiting magnitude of this field should typically be $\gtrsim$1 mag deeper than the limiting magnitude of the SN search images in order to reach equivalent depth for the extended galaxies and the point-source SNe. A natural way of obtaining a deep background field is to add the images from the subsequent search epochs.

When calculating the galaxy properties, we are here primarily interested in the host galaxies of SNe Ia. Therefore, we include all types of galaxies, even though only SNe Ia have been found to occur in elliptical galaxies (e.g., Wang, Höflich, & Wheeler 1997).

The accuracy of redshift determination by using host galaxy magnitude and colors depends on the limiting magnitude, the accuracy in the photometry, and the choice of filters and is a trade-off between the required precision in redshift and the amount of observing time available.

3.1. One Filter

The host galaxy magnitude in the band where the SN search is conducted can be used to calculate a rough probability of the SN being at high z. To quantify this, we estimate the redshift distribution of galaxies as a function of the observed I-band magnitude. We simulate the field by distributing galaxies over a redshift range $0 < z < 2$, with absolute magnitudes according to a field luminosity function (LF). We choose an LF described by two Schechter functions (Schechter 1976), one for early-type galaxies with $M_B^* = -20.2$ and $\alpha = -0.8$ and one for late-type galaxies with $M_B^* = -20.6$ and $\alpha = -1.25$. These values are consistent with results from Metcalfe et al. (1991). Note, however, that the uncertainties in these parameters, especially M_B^*, are fairly large, and it is not clear whether early

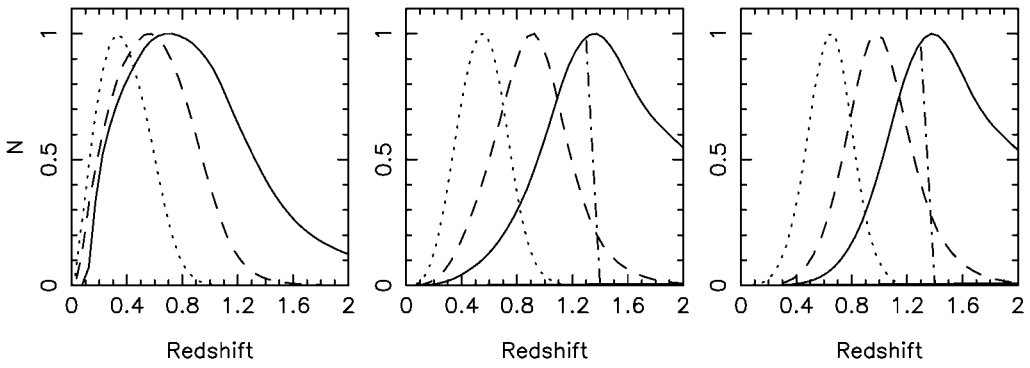

FIG. 2.—*Left:* Redshift distribution of field galaxies in three different magnitude intervals, $20 < m_I < 21$ (*dotted line*), $22 < m_I < 23$ (*dashed line*), and $24 < m_I < 25$ (*solid line*). *Middle:* Redshift distribution of SN host galaxies. Here we have weighted each galaxy with its intrinsic *B*-band luminosity in order to take into account that bright galaxies have a higher probability of hosting an SN. *Right:* Distribution of SN host galaxies, where we assume an evolving SN rate with redshift. The dot-dashed line represents a high-*z* cutoff at $z \sim 1.4$, since in an $m_I \lesssim 25$ search, SNe are too faint to be detected at higher redshifts. Therefore, there should be no host galaxies beyond this cutoff. The peak in each distribution is normalized to unity.

types or late types have the brightest M_B^* (e.g., Metcalfe et al. 1991; Lilly et al. 1995; He, Zou, & Zhang 2000). It is also expected that the LF evolve with redshift (Lilly et al. 1995). At first we do not include a luminosity evolution but take this into account later.

The two Schechter functions are normalized so that the fraction of early-type galaxies is 15%. The late-type galaxies are further divided so that 35% of the total number of galaxies are spirals and 50% irregulars. These are approximately the same fractions as for galaxies in the Hubble Deep Field (HDF) to $z \sim 1$ (Fernándes-Soto, Lanzetta, & Yahil 1999).

Observed magnitudes are calculated by adding the distance modulus and type-dependent *K*-corrections to the rest-frame magnitudes. *K*-corrections are calculated from the E, Sbc, Scd, and Im galaxy templates in Coleman, Wu, & Weedman (1980). We also include an Sa template from Kinney et al. (1996). In the left panel of Figure 2 we plot the resulting redshift distribution for three magnitude bins, $m_I = 20$–21 (*dotted line*), $m_I = 22$–23 (*dashed line*), and $m_I = 24$–25 (*solid line*). The mean redshifts in these bins are $\bar{z} = 0.38$, 0.59, and 0.75, respectively. The percentages of galaxies with redshift $z > 0.85$ are 0.6%, 18%, and 39%, respectively. Without any additional information, these results indicate that a host galaxy should have $m_I > 24$ in order to have a reasonably high probability of being at high redshift. Note that the peak in each distribution in Figure 2 is normalized to unity.

Next we take into account that SNe should be more frequent in galaxies with high intrinsic luminosity. We do this by weighting each galaxy with its rest-frame *B*-band luminosity. For SNe Ia, with the unknown time delay between star formation and SN explosion, the relation between galaxy luminosity and SN rate is probably more complex than a pure proportionality. However, observations show that Type Ia SN rates, as well as Type II rates, are close to proportional to the *B*-band luminosity (Cappellaro et al. 1993). Therefore, in order to compensate for galaxy luminosities, we use the assumption that SNe Ia rates are proportional to *B*-band luminosities.

In the left panel of Figure 3 we show the resulting probability distribution for host galaxy absolute magnitudes. The solid line shows the total distribution, while the dashed and dotted lines show the distribution divided into early-type and late-type galaxies, respectively. The most probable host galaxy magnitudes lie in a range of $\Delta M\pm \sim 1.5$ mag from M_B^*. Note also that the shape of the LF creates a sharp cutoff at bright magnitudes. This can be used in a first rejection of host galaxies based on their apparent magnitudes. For example, a galaxy with apparent magnitude $m_I \sim 20$ would have to have $M_B \lesssim -22.5$ in order to be at $z \gtrsim 0.8$, which according to the plot is unlikely. A strongly evolving LF could, however, move this cutoff to brighter magnitudes. In the right panel of Figure 3 we plot M_B as a function of redshift for a galaxy with observed magnitude $m_I = 20$, for five different galaxy types. The choice of magnitude, $m_I = 20$, is arbitrary here; the plot can be scaled to any apparent *I*-band magnitude.

Using the probability function for host galaxy magnitudes, we plot the redshift distribution of SN host galaxies in the middle panel of Figure 2, using the same magnitude intervals as above. The distributions are here shifted toward higher redshift compared to the left panel. This is natural since intrinsically bright galaxies can be detected to higher redshifts. We must also consider that SNe are not likely to be detected at $z \gtrsim 1.4$ in optical searches to $m_I \sim 25$ (shown in a later section). Therefore, we may safely neglect host galaxies at these redshifts. To compensate for this we introduce a linear cutoff between $z = 1.3$ and $z = 1.4$, as illustrated by the dot-dashed line in Figure 2. The mean redshifts in the three magnitude intervals, $m_I = 20$–21, 22–23, and 24–25, are $\bar{z} = 0.54$, 0.87, and 1.06, respectively. The percentages of probable host galaxies

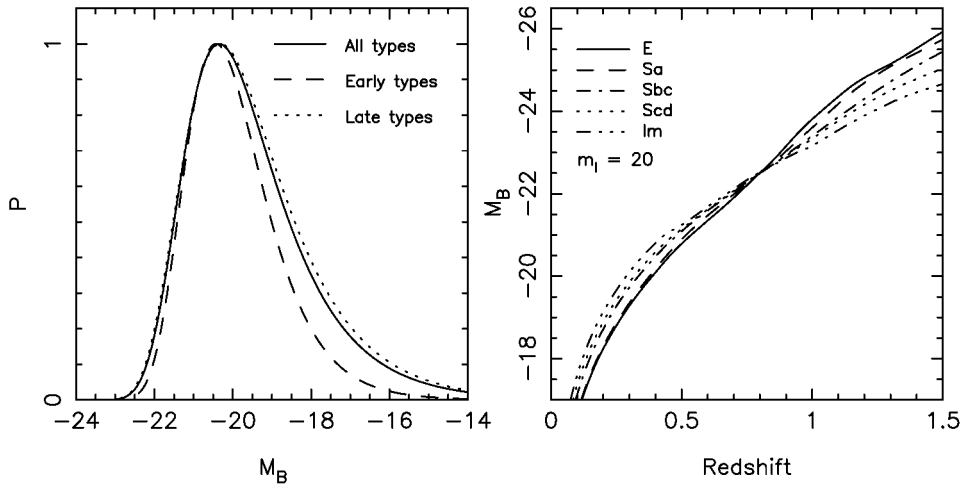

FIG. 3.—*Left:* Probability distribution of SN host galaxy absolute magnitudes in the *B* band. The solid line shows the average probability for all galaxy types, while the dashed and dotted lines show the probability for early types and late types separately. The distributions are derived by weighting the *B*-band luminosity function with the intrinsic luminosity at each magnitude. Peaks are normalized to unity. *Right:* M_B as a function of redshift for a galaxy with observed apparent magnitude $m_I = 20$, for five different galaxy types.

with $z > 0.85$ are 3%, 54%, and 82% for the three magnitude bins, indicating that $m_I \sim 22$ should be sufficiently deep for a relatively high probability of a host galaxy being at high *z*.

So far we have used a nonevolving LF, which here is equivalent to assuming a constant SN rate with redshift. Next we take the increase in galaxy luminosity at high *z* into account by using an evolving Type Ia SN rate ($\tau = 1$ Gyr model from Dahlén & Fransson 1999). The resulting host galaxy distribution is shown in the right panel of Figure 2. Here there is a small shift toward higher redshifts compared to the case with constant SN rate. The mean redshifts in the three magnitude intervals are now $\bar{z} = 0.64$, 0.96, and 1.12. The fractions of host galaxies with $z > 0.85$ in the three bins are 9%, 70%, and 90%, respectively.

In Figure 4 we plot the probability that a host galaxy has a redshift $z > 0.75$ (*dotted line*), $z > 0.85$ (*solid line*), and $z > 0.95$ (*dashed line*), as a function of apparent *I*-band magnitude. The host galaxies are here weighted with their intrinsic luminosities as above. We have used a constant SN rate in the left panel and an evolving rate in the right panel.

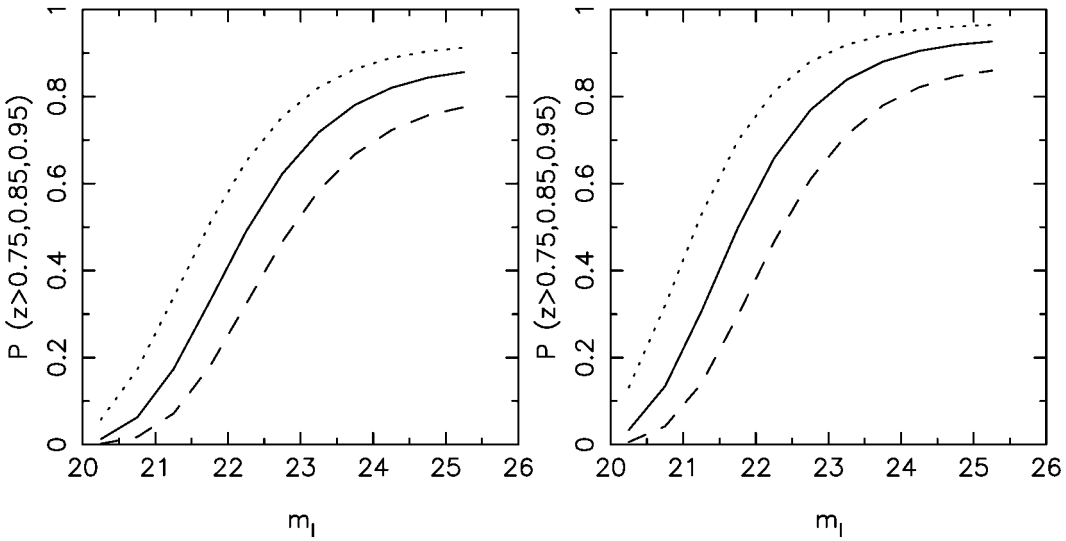

FIG. 4.—Probability that an SN host galaxy has $z > 0.75$ (*dotted line*), $z > 0.85$ (*solid line*), and $z > 0.95$ (*dashed line*) as a function of observed *I* magnitude. *Left:* Case for a constant SN rate. *Right:* Case for an SN rate that evolves with redshift.

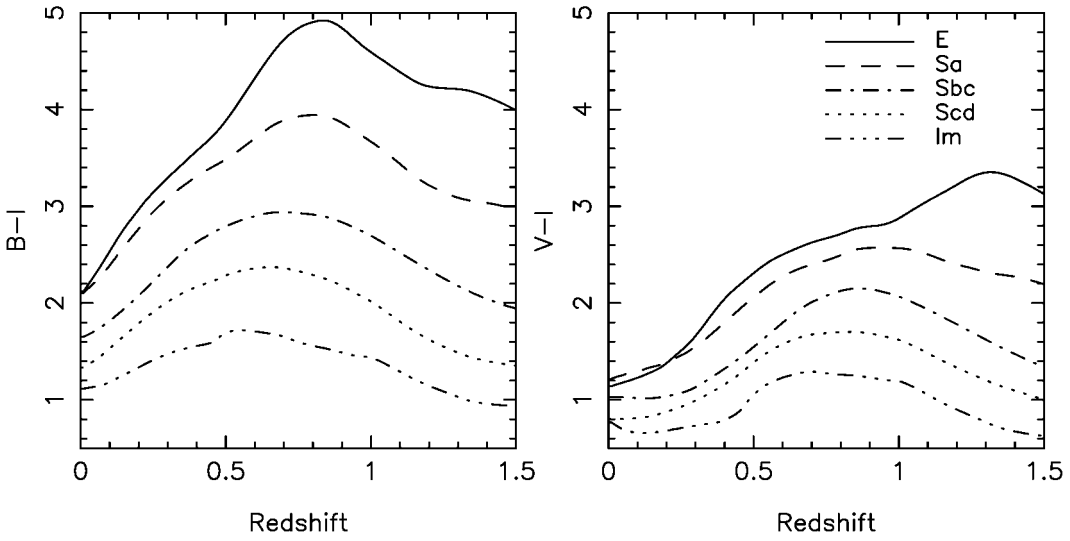

FIG. 5.—$B-I$ and $V-I$ color as a function of redshift for five different types of galaxies.

In the following discussion of host galaxy colors it is important to take into account these results regarding the apparent magnitudes when the redshifts of SN host galaxies are estimated.

3.2. Two Filters

With two filters we can use the color information of the host galaxy together with the apparent magnitude to better constrain the redshift. In addition to the I band, here we assume that B- or V-band magnitudes are available. Figure 5 shows $B-I$ and $V-I$ colors as a function of redshift for the five different galaxy types. The figure clearly illustrates the strong evolution of the galaxy color with redshift. The main reason for the reddening with z is the cosmological shift of the 4000 Å break out of the B and V bands at increasing redshift. At $z \sim 1$ the 4000 Å break moves into the I band, and the curves flatten. The stronger break in early-type galaxies leads to a more pronounced color evolution in E and Sa galaxies. A problem when using a single color is the large spread between different galaxy types. Morphological information on the host galaxy makes the selection efficiency better, even though one should remember that there is no one-to-one correspondence between the morphological type and the spectroscopic type giving the colors (e.g., Dressler et al. 1999; Poggianti et al. 1999). In addition, the presence of internal reddening can affect the colors of a specified morphological type. Therefore, one should be careful when using a single color to estimate redshift.

Note also that the evolution is generally stronger in $B-I$. However, this also leads to a rapid faintening of the galaxies in B, and long exposure times are needed in order to measure the colors.

3.3. Three Filters

When the galaxy spectrum is cosmologically redshifted, the colors change, as described in the previous section. This effect can be quantified by the evolution of observed colors in a color-color diagram. The left panel of Figure 6 shows the position of galaxies (E, Sa, Sbc, Scd, and Im) in a two-dimensional color-color diagram of $B-R$ versus $R-I$, while the right panel shows the same for $V-R$ versus $R-I$. The crosses define the $z = 0$ position for each galaxy type. The contours show the color-color evolution up to $z = 1.2$, marked by open circles, where steps in z of 0.2 are shown by vertical bars.

Note that marks defining the same redshifts approximately fall on straight "isoredshift" contours going from the bottom left to the top right part of the figures. Including a larger sample of templates with intermediate types results in color-color curves with redshift marks approximately falling on these contours. Including internal reddening in the templates also shifts the curves along the isoredshift contours. For example, assuming that $E(B-V) = 0.3$ in an Scd galaxy makes the colors become almost identical to those of an Sbc galaxy. Internal reddening is therefore not a severe problem when redshifts are estimated using color-color selection.

As can be seen in the plot, the bottom right part defines a region with $z \gtrsim 0.85$. Note also that using B instead of V results in a more distinct evolution (note different scales on the y-axis). As already mentioned, however, the trade-off with the B band is that significantly more observing time is required. We discuss this in § 4.

One should notice that there are many factors involved when using color-color selection, i.e., filter choices, magnitude limits, accuracy in magnitudes, the galaxy types of interest, and their absolute magnitudes. To quantify how three-filter color-color

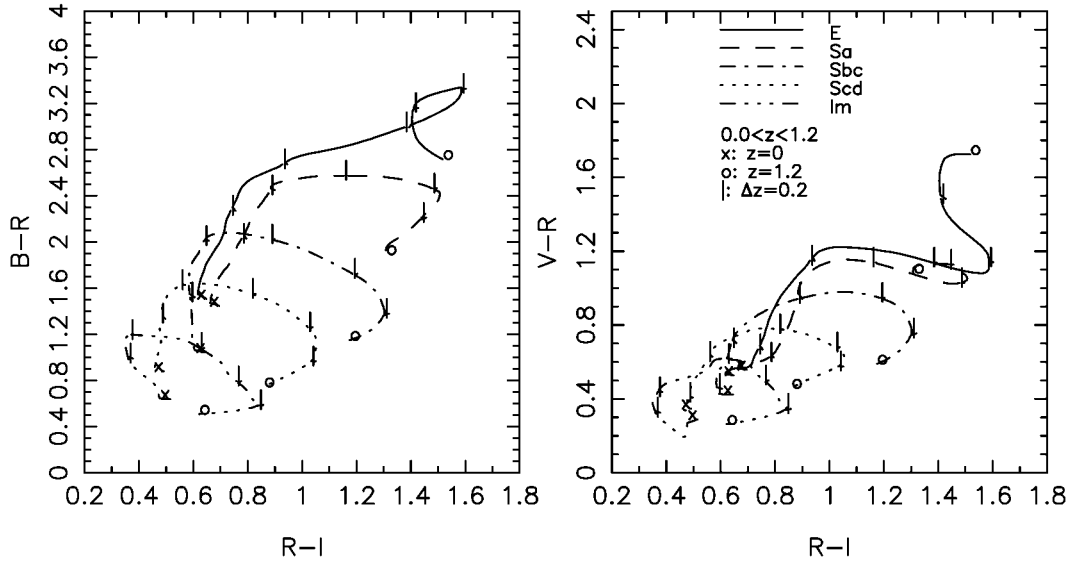

FIG. 6.—*Left:* Evolution of the $V-R$ vs. $R-I$ color-color diagram with redshift for five different galaxy types. *Right:* Same but for $B-R$ vs. $R-I$. High-*z* galaxies occupy the bottom right part of the plot.

selection can be used in order to select high-*z* candidates, we use MC simulations. In the example we choose to select host galaxies with $z \geq 0.85$. For this redshift limit, *R* and *I* filters should be used, since here the 4000 Å break has just left the *R* band and is moving into the *I* band. In the simulations, both the *B* and *V* bands are used as the third filter. The *U* band has not been considered because of the long exposure times that would be needed in that case.

3.3.1. Color-Color Selection with BRI and VRI

A total of ~250,000 galaxies were generated and distributed from early-type elliptical galaxies to irregulars, with a distribution according to the LF described in § 3.1 and in a redshift range $0 < z < 1.4$. Observed magnitudes are calculated by adding distance modulus and type-dependent *K*-corrections. To each magnitude (i.e., *B*, *V*, *R*, and *I*) of each galaxy, a random

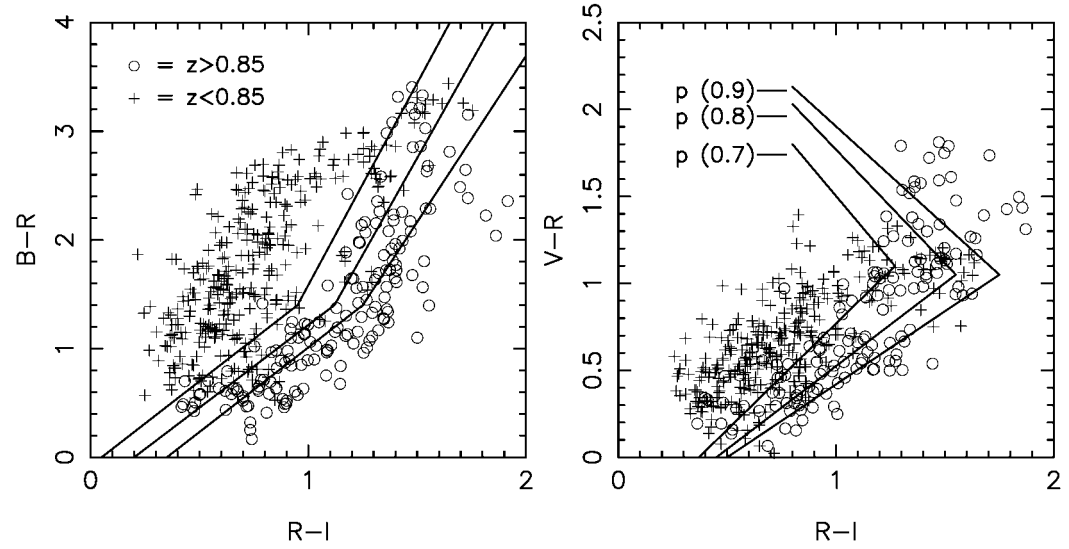

FIG. 7.—*Left:* Color-color selection criteria in $B-R$ vs. $R-I$. Plus signs represent galaxies with $z < 0.85$, and circles galaxies with $z > 0.85$. On the right side of the lines the probability that a host galaxy has $z > 0.85$ is 0.7 (*left line*), 0.8 (*middle line*), and 0.9 (*right line*). *Right:* Same but for $V-R$ vs. $R-I$.

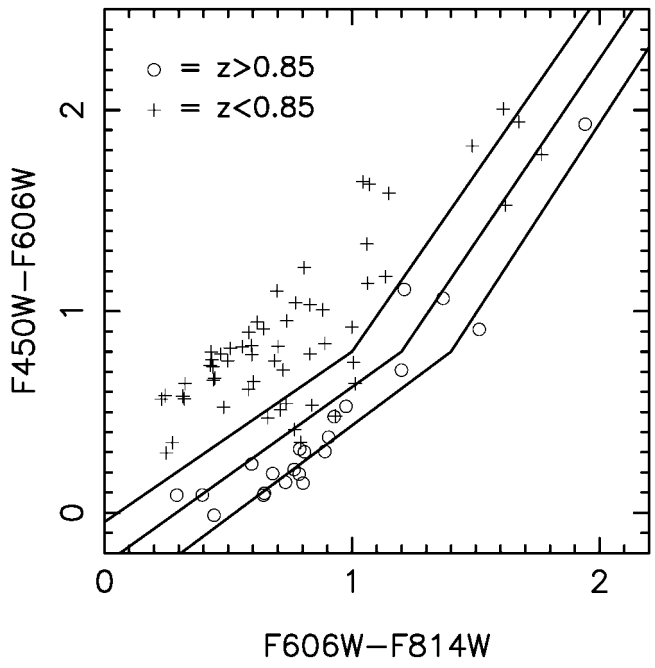

FIG. 8.—Color-color selection criteria for the HDF calculated from MC simulations. To the right of the three lines the probabilities are (*from left to right*) 0.7, 0.8, and 0.9 that a galaxy has $z > 0.85$. Galaxies in the HDF with spectroscopic redshift $0.85 < z < 1.4$ are marked by circles, while galaxies with $z < 0.85$ are marked by plus signs. Spectroscopic and photometric data for the HDF are taken from Fernándes-Soto et al. (1999).

error is generated so as to mimic the real uncertainties in photometry. We use a normal distribution with a σ-value varying from 0.06 mag at bright magnitudes, $m_I < 20$, to 0.1 mag at our limit $m_I = 25$. Besides the variation in colors due to spectral type and internal reddening, there is also a possibility of an intrinsic variation in the colors within a specified spectral type. To account for this we add an extra dispersion of 0.1 mag to each color. This is consistent with the difference in colors between the template sets of Coleman, Wu, & Weedman (1980) and Kinney et al. (1996) when elliptical and Sbc galaxies are compared individually. We distribute galaxies out to the cutoff at $z \sim 1.4$, described in § 3.1. We consider two models with different SN rates. The first model has a constant SN rate, equivalent with a nonevolving LF. In the second model we weight each galaxy with the SN rate taken from the evolving model with $\tau = 1$.

Figure 7 shows a representative fraction of the generated galaxies in color-color diagrams in the case of a nonevolving LF. The circles represent galaxies with redshift $z > 0.85$; crosses show the galaxies with $z < 0.85$. Three lines are also shown in the figure as examples of selection criteria. On the right side of these lines the probability that a host galaxy has $z > 0.85$ is 0.7, 0.8, and 0.9 for the left, middle, and right lines, respectively. In the following we call these probability criteria $p_{(0.7)}$, $p_{(0.8)}$, and $p_{(0.9)}$. As expected, these criteria are almost parallel to the isoredshift contours for $z \sim 0.85$. Therefore, using a larger set of templates or including internal reddening does not affect the results since this mainly moves the galaxy colors along these contours.

The difference in selection efficiency between using B and V can be quantified by calculating the fraction of the simulated galaxies with known redshift $z > 0.85$ that are actually picked out by the selection criteria. With *BRI* selection, (40%, 64%, 86%) of the galaxies that have $z > 0.85$ are picked out when ($p_{(0.9)}$, $p_{(0.8)}$, $p_{(0.7)}$) is used. With *VRI* selection, the numbers are (31%, 47%, 73%). For the model with evolving SN rate, there are relatively more SNe at high z; therefore, the selection efficiency is higher in this model. We find that (51%, 86%, 99%) of the galaxies that have $z > 0.85$ are picked out when we construct selection criteria ($p_{(0.9)}$, $p_{(0.8)}$, $p_{(0.7)}$) in *BRI*. With *VRI*, the percentages are (43%, 80%, 98%).

Similar selection criteria can easily be produced for other choices of redshift, filters, photometric errors, and limiting magnitudes. Note that it is important that the selection criteria be calculated for a limiting magnitude matching that of the real observations. For example, if the limiting magnitude is $m_I = 22$, instead of $m_I = 25$ as used here, then the lines representing the 0.9 probability criterion in the plot will no long-

TABLE 1
REST-FRAME B MAGNITUDES AS A FUNCTION OF REDSHIFT FOR FIVE DIFFERENT GALAXY TYPES, ASSUMING AN OBSERVED MAGNITUDE $m_I = 25$

z	E (mag)	Sa (mag)	Sbc (mag)	Scd (mag)	Im (mag)	$f(m_I = 24)$	$f(m_I = 25)$	$f(m_I = 26)$
0.8	−17.5	−17.5	−17.5	−17.5	−17.5	0.80	0.91	0.96
0.9	−18.1	−18.0	−17.9	−17.9	−17.8	0.73	0.87	0.94
1.0	−18.8	−18.6	−18.4	−18.3	−18.1	0.63	0.82	0.92
1.1	−19.3	−19.2	−18.8	−18.7	−18.5	0.51	0.75	0.88
1.2	−19.8	−19.7	−19.3	−19.1	−18.9	0.40	0.67	0.84
1.3	−20.1	−20.1	−19.7	−19.5	−19.2	0.30	0.58	0.79
1.4	−20.5	−20.4	−20.1	−19.8	−19.4	0.22	0.50	0.74

NOTE.—The last three columns list the fraction of the SN host galaxies that can be detected at the different redshifts for three limiting magnitudes, $m_I = 24$, $m_I = 25$, and $m_I = 26$.

TABLE 2
APPARENT MAGNITUDES IN DIFFERENT FILTERS FOR GALAXIES AT DIFFERENT REDSHIFTS, WHEN THE OBSERVED MAGNITUDE IS $m_I = 25$

	Elliptical Galaxy			Sbc Galaxy			Irr Galaxy		
z	m_B (mag)	m_V (mag)	m_R (mag)	m_B (mag)	m_V (mag)	m_R (mag)	m_B (mag)	m_V (mag)	m_R (mag)
0.8	29.9	27.7	26.6	27.9	27.1	26.2	26.6	26.3	25.8
0.9	29.8	27.8	26.5	27.8	27.1	26.3	26.5	26.2	25.8
1.0	29.6	27.9	26.4	27.7	27.1	26.3	26.4	26.2	25.8
1.1	29.4	28.1	26.4	27.5	26.9	26.3	26.3	26.0	25.7
1.2	29.2	28.2	26.5	27.3	26.8	26.2	26.1	25.9	25.6
1.3	29.2	28.4	26.8	27.2	26.6	26.1	26.0	25.8	25.5
1.4	29.1	28.3	26.9	27.0	26.5	26.0	26.0	25.7	25.4

er be valid. Instead, these lines would represent a ~0.6–0.7 probability.

Note also that the apparent magnitudes for the individual galaxies are not explicitly used in the color-color selections (except that they must be brighter than the limiting I magnitude). Therefore, one should take the results regarding the absolute magnitudes of the host galaxy into account, e.g., the results described by Figure 3.

3.3.2. Checking the Simulation against HDF

To test the color-color selection against real observations, we calculate selection criteria for the HDF-N using MC simulations as above, using a constant SN rate. We use the F450W, F606W, and F814W filters, corresponding to *B*, *V*, and *I*. In Figure 8 we plot selection criteria analogous to Figure 7, i.e., to the right of the three lines the probabilities are 0.7, 0.8, and 0.9 (*from left to right*) that a host galaxy has $z > 0.85$. In the figure we have also plotted galaxies in the HDF with spectroscopic redshift $0.0 < z < 1.4$ and $m_I < 25$. Photometry and redshifts for these galaxies are taken from the catalog published by Fernández-Soto et al. (1999). Galaxies with spectroscopic redshift $z > 0.85$ are marked by circles, while lower redshift galaxies are marked by crosses. In total there are 79 galaxies to the limiting magnitude, of which 22 are at $z > 0.85$. The figure shows that the high-z and low-z galaxies occupy different regions in the color-color plot. To the right of the $p_{(0.7)}$ line, 65% of the real galaxies have $z > 0.85$. For the $p_{(0.8)}$ and $p_{(0.9)}$ lines, 80% and 100% of the galaxies have $z > 0.85$. Of the total number of galaxies with $z > 0.85$, 100% lie to the right of $p_{(0.7)}$, while 91% and 36% lie to the right of $p_{(0.8)}$ and $p_{(0.9)}$, respectively.

3.4. Four or More Filters

With a set of four or more filters available, it is possible to set *both* lower and upper limits on the redshifts of individual galaxies, using photometric redshift techniques (as compared to the three-filter case, where we estimate the probability that a galaxy has a redshift above, *or* below, some chosen limit). The photometric redshift technique has developed much during recent years and has now been used in a variety of applications. There are basically two different approaches to the technique. In the empirical fitting method (e.g., Connolly et al. 1995, 1997; Wang, Bahcall, & Turner 1998; Brunner, Connolly, & Szalay 1999), a training set of galaxies with known redshifts are used to derive a polynomial giving the redshift as a function of colors and magnitudes. In the template fitting technique (Puschell, Owen, & Laing 1982; Gwyn 1995; Mobasher et al. 1996; Sawicki, Lin, & Yee 1997; Fernández-Soto et al. 1999; Bolzonella, Miralles, & Pelló 2000; Fontana et al. 2000), a χ^2 fit is made between observed colors and a set of galaxy templates red-

TABLE 3
LIMITING MAGNITUDES IN B, V, AND R THAT ARE REQUIRED IN ORDER TO DETECT 70%, 80%, 90%, AND 95% OF THE GALAXIES WITH $m_I \lesssim 25$

	f_{70}			f_{80}			f_{90}			f_{95}		
z	m_B (mag)	m_V (mag)	m_R (mag)	m_B (mag)	m_V (mag)	m_R (mag)	m_B (mag)	m_V (mag)	m_R (mag)	m_B (mag)	m_V (mag)	m_R (mag)
0.8	26.1	25.0	24.3	26.7	25.5	24.7	27.5	26.0	25.2	28.1	26.4	25.6
0.9	26.3	25.4	24.6	27.0	25.8	25.0	27.9	26.3	25.5	28.5	26.8	25.8
1.0	26.4	25.7	24.9	27.2	26.1	25.2	28.1	26.6	25.6	28.6	27.1	25.9
1.1	26.3	25.8	25.1	27.3	26.3	25.4	28.2	27.0	25.7	28.7	27.4	26.0
1.2	26.2	25.8	25.2	27.2	26.4	25.5	28.2	27.2	25.8	28.7	27.7	26.1
1.3	26.0	25.7	25.3	27.0	26.3	25.6	28.2	27.4	26.0	28.8	27.9	26.3
1.4	25.9	25.6	25.3	26.7	26.1	25.5	28.1	27.3	26.2	28.7	27.9	26.6

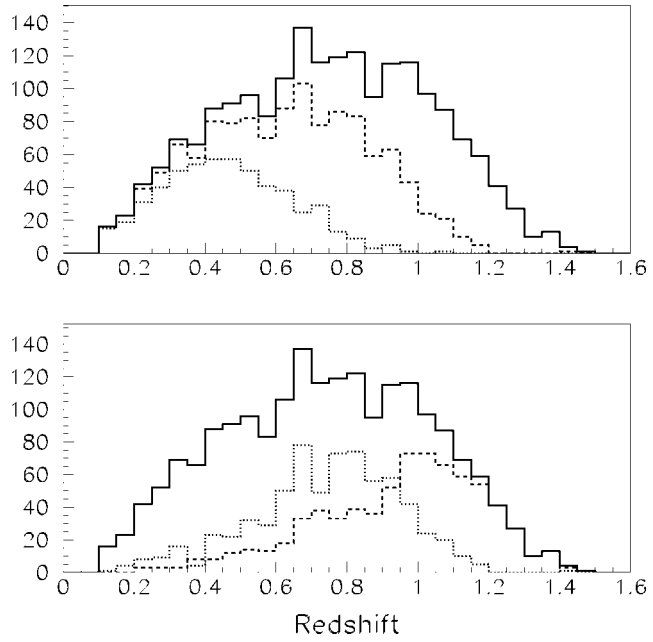

FIG. 9.—Redshift distribution of discovered Type Ia SNe (in arbitrary units), assuming a constant SN rate per comoving volume. A discovery requires that the subtracted SN photometry between the detection and reference images exceed the threshold brightness in the *I* band. On the left-hand side, the redshift distributions are calculated for limiting *I*-band magnitudes, $m_I = 23$ (*dotted line*), 24 (*dashed line*), and 25 (*solid line*), using the SNOC Monte Carlo package (A. Goobar et al. 2002, in preparation). The bottom panel shows also the redshift distribution that arises with magnitude bounds on both sides: $23 < I < 24$ (*dotted line*) and $24 < I < 25$ (*dashed line*).

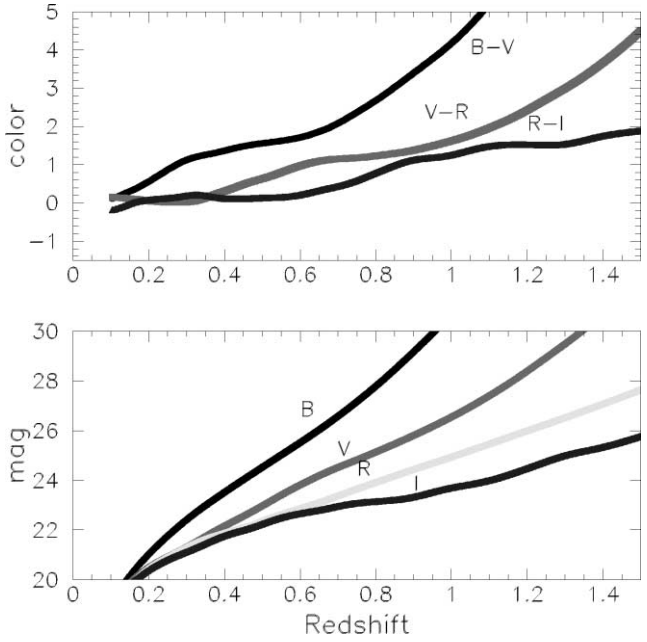

FIG. 10.—Color and magnitude vs. redshift at light-curve maximum for "normal" Type Ia SNe.

shifted over a range of redshifts. The accuracy of the method to $z \lesssim 1.3$ can reach $\sigma_z \sim 0.05(1 + z)$ (Cohen et al. 2000), depending on the number of filters and photometric errors. With this accuracy, high-*z* host galaxies can readily be found. The trade-off with the method is, of course, the large amount of observing time required to map a large sky coverage in at least four bands. A public available code, *hyperz*, for calculating photometric redshifts using the template fitting method is published by Bolzonella et al. (2000).

4. GALAXY MAGNITUDES

In this analysis we have used a limiting magnitude $m_I = 25$. Two questions should be addressed here. Is this deep enough to reach host galaxies at redshifts of interest, and what limiting magnitudes are required in the other filters in order to get the desired colors? In Table 1 we give the rest-frame *B* magnitudes as a function of redshift for different galaxy types, assuming an observed magnitude $m_I = 25$. Comparing these results with Figure 3 shows that most host galaxies at $z \lesssim 1$ should be reached, since we here reach an absolute magnitude $M_B \gtrsim -19$. To quantify this further, we also list the fraction of SN host galaxies that can be detected at different redshifts, assuming three different limiting magnitudes, $m_I = 24$, $m_I = 25$, and $m_I = 26$.

Next we investigate the limiting magnitudes that must be reached in different filters to get the colors of galaxies of different types and at different redshifts. In Table 2 we list the apparent magnitudes in *B*, *V*, and *R* for galaxies with an *observed magnitude* $m_I = 25$. We list the magnitudes for E, Sbc, and Im galaxies. Sa and Scd galaxies have magnitudes approximately in between these.

Note that Table 2 does not imply that galaxies get brighter at higher redshift. If we consider two elliptical galaxies at, e.g., $z = 0.8$ and $z = 1.4$ that have the *same apparent magnitude in the I band*, then the galaxy at $z = 1.4$ will be 0.8 mag brighter in *B* than the galaxy at $z = 0.8$. This is a consequence of the turnover at $z \gtrsim 0.8$ in the $B-I$ color versus redshift diagram (Fig. 5).

Finally, we estimate the limiting magnitudes in *B*, *V*, and *R* that are required in order to detect 70%, 80%, 90%, and 95% of the host galaxies with $m_I \leq 25$, in these three filters, at different redshifts. Results are listed in Table 3. Again, in some bands there is an apparent trend of brighter limiting magnitudes at higher *z*, which is explained by the use of a constant limit on the *I* band. One must here take into account that a decreasing fraction of the total number of host galaxies are detected to this limit in *I*, as shown in the $f(m_I = 25)$ column of Table 1.

It is also important to remember that the fractions given in Table 1 and the magnitudes given in Table 3 are calculated for SN host galaxies, i.e., where we have weighted each galaxy with its intrinsic luminosity. The fractions and magnitudes are therefore not valid for a pure galaxy search.

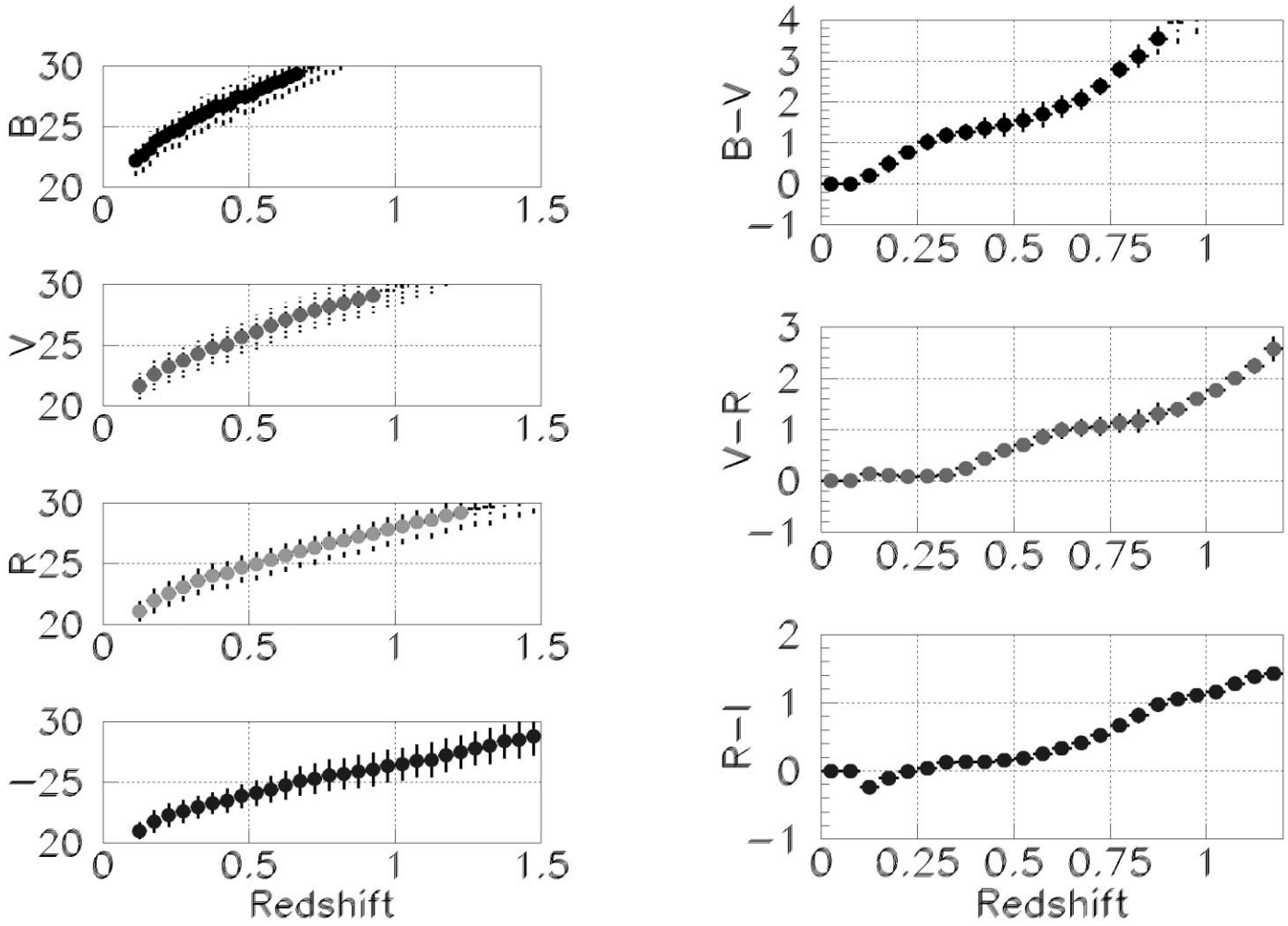

FIG. 11.—*Left, from top to bottom:* Average *BVRI* magnitudes vs. redshift at the discovery epoch. *Right:* Average color vs. redshift at discovery epoch for SN magnitudes $m_I < 25$.

As an example, Table 3 shows that in order to get colors of 90% of the objects at $z \sim 1$, detected in a survey with limiting magnitude $m_I = 25$, it is necessary to reach $m_B \sim 28.1$, $m_V \sim 26.8$, and $m_R \sim 25.6$. This information should be complemented by the results in Table 1, which shows that ~82% of the total number of host galaxies at $z \sim 1$ should be brighter than the limiting magnitude $m_I = 25$. The typical telescope time needed to reach $m_I = 25$ with an 8 m class telescope is ~0.3 hr (1.1 hr) for an S/N = 5 (10). The total time required to get three-color information in *VRI* is ~1.5 hr (6 hr), assuming depths $m_V \sim 27$, $m_R \sim 26$, and $m_I \sim 25$. Adding the *B* band requires an additional 2.2 hr (8.9 hr) of observing time, i.e., more than the other three bands together. Numbers are taken from the Subaru telescope's Suprime-Cam.[1]

[1] Exposure Time Calculator at http://www.subaru.naoj.org.

5. USING SN MAGNITUDE AND COLOR TO ESTIMATE REDSHIFT

Similar to using host galaxy magnitudes and colors, it is possible to use these quantities of the SNe themselves to estimate the redshift and SN type. For example, Riess et al. (2001) concluded that the most distant known SN, SN 1997ff, was a Type Ia SN at a redshift $z = 1.7 \pm 0.1$, based on the SN photometry. From the host galaxy, Riess et al. derived a consistent photometric redshift, $z = 1.65 \pm 0.15$.

One difficulty is the temporal evolution of the SN light: one does not know at which phase in the light curve the SN was discovered. In this section we use the Monte Carlo simulation package SNOC (A. Goobar et al. 2002, in preparation) to compute the SN discovery and selection probabilities using the photometric and spectroscopic templates of "normal" Type Ia SNe described in Nugent, Kim, & Perlmutter (2002). A po-

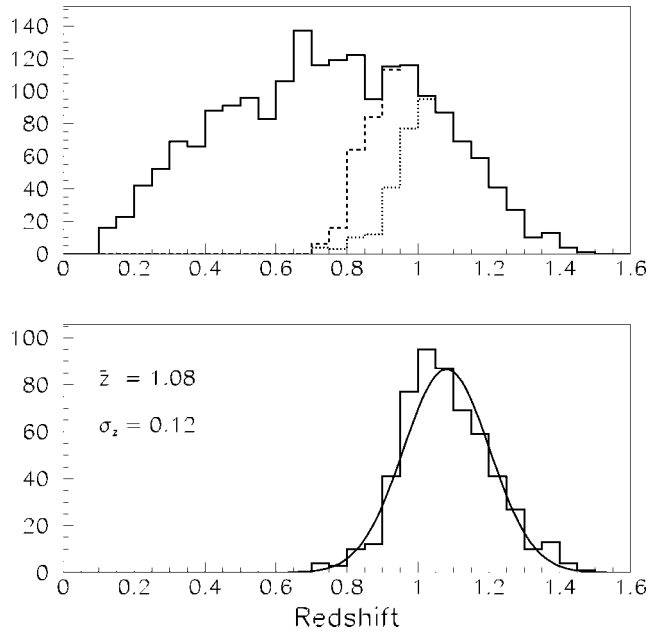

FIG. 12.—*Top:* Selected redshift range with cut on $R-I>0.8$ (*dashed line*) and a combined criterion $R-I>0.8$ and $V-R>1.5$ (*dotted line*). *Bottom:* Gaussian fit to the *z*-distribution imposing both selection criteria. The mean redshift of the selected SNe is $\bar{z}\sim 1.1$, with a deviation $\sigma_z\sim 0.13$ for an assumed color uncertainty (intrinsic+measurement error) of 0.2 mag.

tential selection bias due to color-brightness correlations could be a source of concern but is not considered in this work.

The simulated redshift distribution of the discovered Type Ia SNe in an *I*-band search is shown in the upper panel of Figure 9. To produce a conservative estimate of the number of SNe with redshift $z>1$, we have assumed that the SN rate per comoving volume is constant up to $z\sim 1.5$.

In the simulations, SNe are selected when the subtraction of SN photometry 3 weeks apart exceeds the threshold brightness in the *I* band, e.g., $m_I<25$.[2] The absolute peak magnitude of the Type Ia SNe is assumed to be $M_B=-19.33$, with an intrinsic spread of $\Delta M_B^{\rm rest}=0.40$ mag. This large spread gives a conservative representation of the distribution of brightness for SNe Ia to any light-curve shape corrections. The intrinsic brightness spread at discovery is further enlarged by the wide range of possible SN light-curve phases.

For simplicity, we have assumed that all the SNe have the same light-curve shape, i.e., constant "stretch" (or Δm_{15}).

As discussed earlier, Type Ia SNe are found in a very broad redshift range if the selection of candidates is set by a threshold on the SN *I*-band magnitude alone. One way to narrow down the distribution is to impose a lower cutoff on the candidate's brightness. However, this may not be sufficiently efficient as shown in the bottom panel of Figure 9, where we plot the redshift distribution of SNe in 2 mag intervals, $23<m_I<24$ and $24<m_I<25$. Long tails toward the lower redshifts make this approach not optimal. In addition, this sort of criterion is likely to introduce a selection bias, which could severely worsen the precision of cosmological parameters to be estimated from the data set and the measurements of the SN rates. Next, we investigate the brightness and colors of Type Ia SNe versus redshift. Figure 10 shows the optical color and magnitude evolution at the date of maximum for the redshifted rest-frame *B*-band light of a "normal" Type Ia SN.

We use SNOC to study the magnitudes and colors of the SNe at the discovery epoch assuming a 3 week gap between reference and discovery images. Figure 11 shows the *average* magnitude and its standard deviation in *BVRI* and the $B-V$, $V-R$, and $R-I$ color at the discovery epoch. Note that the intrinsic spread in the SN peak magnitude, as well as the measurement errors, are small compared to the magnitude range that emerges from all the possible reference and discovery epochs for the SNe.

5.1. Two- and Three-Band Selection

Next we show examples of possible selection criteria using two and three filters. Figure 12 shows the selected range of redshifts demanding $R-I>0.8$ (*dashed line*) and *in addition* demanding $V-I>1.5$ (*dotted line*). The solid line shows the total distribution of Type Ia SNe with $m_I\leq 25$. We assume an uncertainty in the color from both intrinsic color dispersion and measurement Gaussian error of $\sigma_M=0.1$ mag. In the bottom panel we fit a Gaussian probability density function to the redshift distribution of SNe after imposing both criteria. This fit shows that it is possible to select candidates around $z\sim 1$ with an accuracy $\sigma_z\approx 0.12$ if three bands are used. The *VRI* selection rejects about 73% of the detected SNe, but it is 82% (99%) efficient in keeping candidates with $z\geq 0.9$ ($z\geq 1.0$). Of the selected sample, less than 6% (27%) are below $z=0.9$ ($z=1.0$).

If the selection is done based solely on $R-I$, 41% of the detected SNe are kept and the width of redshift distribution is $\sigma_z\approx 0.15$. The selection efficiency becomes nearly 100% for $z\geq 0.9$. The fraction of selected SNe below $z=0.9$ ($z=1.0$) is then 21% (49%). Thus, the *V*-band information does help in rejecting the lower redshift SNe tail while introducing a moderate decrease in overall efficiency. Given the faintness of $z>1$ SNe in the *V* band, $V\gtrsim 27$ mag, a simple $R-I$ selection might be adequate in a realistic scenario.

Finally, we address the issue of non-Ia SN contamination. Figure 13*a* shows the simulated redshift distribution of discovered Type Ia (*solid line*) and core-collapse (*dashed line*) SNe for a 3 week image separation search with limiting magnitude $m_I<25$. The non-Ia SNe were simulated in the same way as Type Ia SNe. All SN types were assumed to have a constant rate per comoving volume in the considered redshift range. The adopted relative intrinsic rate was $N_{\rm Ia}/N_{\rm core}=1/2.6$ for $z<1.6$. Within the non-Ia class, the various SN types (Ib/c, IIL, IIn, IIP, 87a-like) were given absolute peak magnitudes, disper-

[2] The selection criterion is thus not identical to the one described in § 2.

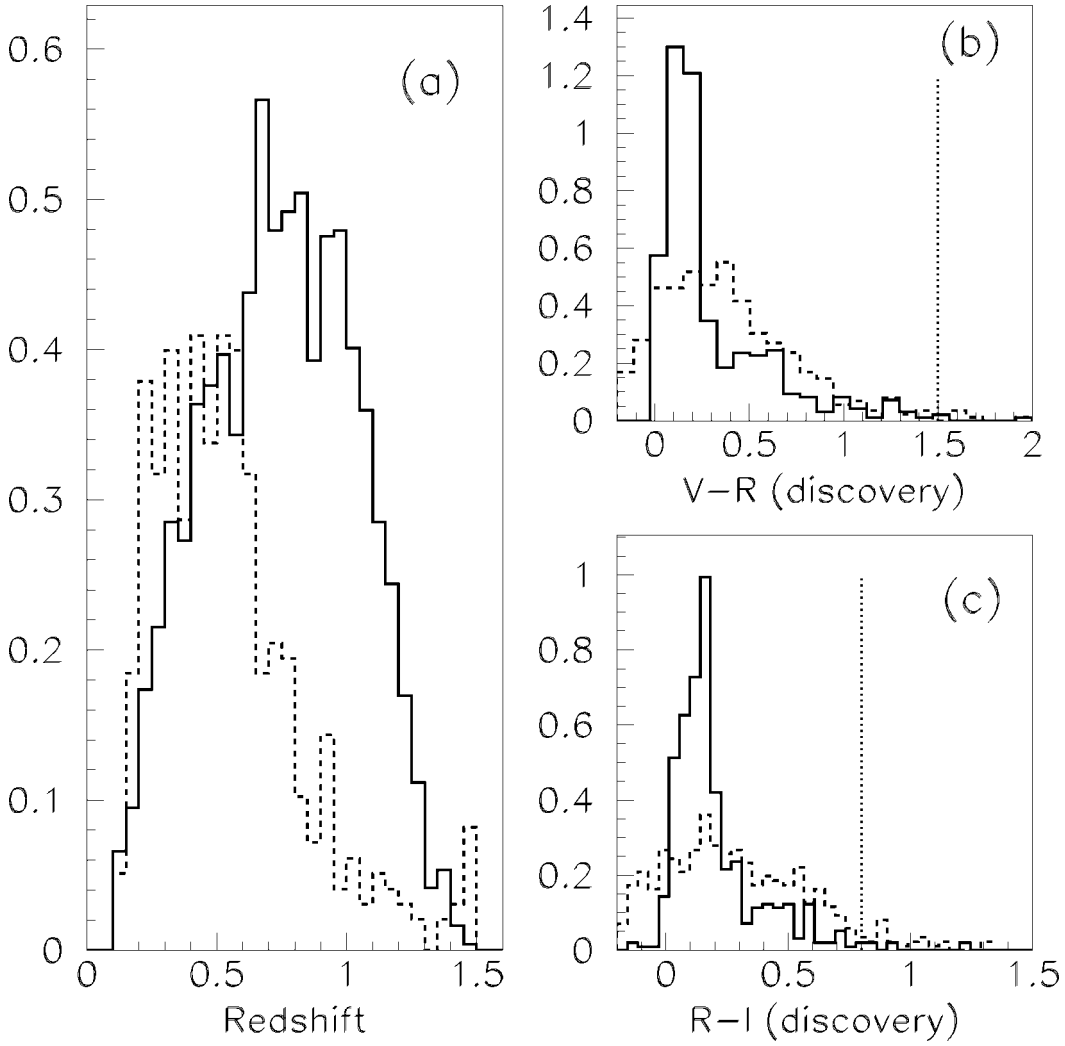

FIG. 13.—(*a*) Redshift distribution of observable Type Ia SNe (*solid curves*) compared to the non-Ia SN contamination (*dashed curves*) for an SN search with limiting magnitude $m_I < 25$ (units are arbitrary). (*b*) $V-R$ color at the discovery epoch for the selected non-Ia SNe. The dashed curves include a 0.3 mag uncertainty from either measurement error or intrinsic dispersion. The dotted line shows the adopted color selection $V-R > 1.5$. (*c*) $R-I$ at the discovery epoch for the non-Ia simulated SNe. The dotted line shows the selection criterion $R-I > 0.8$.

sions, and relative fractions according to Table 1 in Dahlén & Fransson (1999). For dust extinction by the SN host galaxy, we assume a face-on value $A_{B0} = 0.32$. Inclination effects are taken into account by adding an extinction $A_{Bi} = 0.32[(\cos i)^{-1} - 1]$, where a random inclination i is assigned to each object.

The type of search we simulated produces a non-Ia candidate for every two Type Ia SNe found.[3] Figures 13*b* and 13*c* show how the adopted color selections, $V-R > 1.5$ and $R-I > 0.8$ (and $m_I < 25$), discriminate against the non-Ia SNe, leaving a negligible contamination rate, even when a 0.3 mag uncertainty in color from either measurement or intrinsic dispersion is added (*dashed curves*).

6. SUMMARY AND CONCLUSIONS

We have shown that deep wide-field SN searches will detect a number of SNe over a broad redshift range. For example, an optical search to $m_I \sim 25$ will find Type Ia SNe to $z \sim 1.5$. In this paper we discuss the use of magnitudes and colors of the SNe, as well as the host galaxies, in order to make a prompt selection of high-*z* SN candidates, for subsequent spectroscopic follow-up. We first discuss the use of additional photometric information on the host galaxies. The advantage of using the host galaxies for redshift estimates is that a catalog of high-*z*

[3] This number is rather sensitive to the limiting magnitude adopted. For example, for a limiting magnitude $m_I < 23$, one expects only one non-Ia SN for every five SNe Ia assuming constant rate per comoving volume for all SN types.

candidate galaxies can be constructed in advance, enabling a direct selection once an SN is discovered.

Using the available magnitude information in the search filter gives a first indication of the probability that an SN is at high z. Adding broadband filters increases the probability for a correct selection. Because of the cosmological shift of galaxy spectra, galaxies appear redder when they are at higher redshift (in optical to $z \sim 1$). Using the color from two filters, together with the magnitude information, one can therefore set additional constraints on the redshift of the galaxy. Note, however, that different galaxy types have different colors, as well as evolution in color, which makes a single color difficult to use. The selection efficiency increases if the galaxy type is known; however, one must remember that there is no one-to-one relation between morphological type and colors.

If observations of the host galaxies are available in three filters, then it is possible to derive selection criteria from the position of the galaxy in a color-color diagram. As an example, we show how such criteria can be constructed to select host galaxies with $z > 0.85$. Using *B*, *R*, and *I* photometry, we construct a selection criterion so that the probability is 80% that a galaxy has $z > 0.85$ and where ~64%–86% of the total number of host galaxies above this redshift are actually selected. By changing the selection criterion, we can increase the probability that the host galaxy is at high z; this will, however, lead to a decrease of the fraction of the total number of high-z host galaxies that are selected.

With four or more available filters it is possible to estimate the photometric redshift of the host galaxies. This results in an estimate of the redshift for each galaxy separately, as compared to the three-filter case, where we instead calculate the probability that a host galaxy has a redshift above, or below, some chosen limit.

We also discuss the necessary depth of a search in order to detect host galaxies at $z \sim 1$ and the depths required in other filters in order to calculate colors. From the results listed in Tables 1 and 3, we see that with a limiting magnitude $m_I = 25$, about 80% of the host galaxies at $z \sim 1.0$ can be detected, while at $z \sim 1.3$ the fraction is ~60%. The required depths in the other optical filters to detect 90% of the galaxies with $m_I = 25$ are $m_B \sim 28.1$, $m_V \sim 26.8$, and $m_R \sim 25.6$.

In a similar way, we show that the colors of the Type Ia SNe can also be used to constrain the redshift. A selection criterion based on $(V)RI$ magnitudes in an SN search with limiting magnitude $m_I \sim 25$ leads to a possible narrowing of the redshift range of the candidates to $\sigma_z \leq 0.15$ at $z \sim 1$. Here 30%–40% of the total number of SNe are selected, of which 75%–90% have $z > 0.9$. Multiband photometry of SNe is also very useful to distinguish between SNe of different types.

Selections based on the host galaxy magnitude and colors are preferable because they are less likely to introduce selection biases. In addition, obtaining colors of the SNe requires deep multiband observations of each candidate taken within a relatively short time interval, making this technique less feasible.

More observational data are needed in order to understand and quantify the possible color-brightness correlation of high-z SNe and the resulting selection bias.

Finally, the accuracy of the redshift determination, from both the galaxy and SN photometric information, depends on several parameters: depths, number of available filters, accuracy in photometry, etc., and is a trade-off between required accuracy and the amount of observing time available.

We wish to thank the anonymous referee for valuable comments and suggestions. We also thank Peter Nugent for providing us with spectral templates of Type Ia SNe. We are grateful to Saul Perlmutter and Göran Östlin for useful discussions. The work by T. D. is supported by the Swedish Research Council and the Swedish Board for Space Sciences. A. G. is a Royal Swedish Academy Research Fellow supported by a grant from the Knut and Alice Wallenberg Foundation.

REFERENCES

Bolzonella, M., Miralles, J.-M., & Pelló, R. 2000, A&A, 363, 476
Brunner, R. J., Connolly, A. J., & Szalay, A. S. 1999, ApJ, 516, 563
Cappellaro, E., Turatto, M., Benetti, S., Tsvetkov, D. Yu., Bartunov, O. S., & Makarova, I. N. 1993, A&A, 268, 472
Cohen, J. G., Hogg, D. W., Blandford, R., Cowie, L. L., Hu, E., Songaila, A., Shopbell, P., & Richberg, K. 2000, ApJ, 538, 29
Coleman, G. D., Wu, C.-C., & Weedman, D. W. 1980, ApJS, 43, 393
Connolly, A. J., Csabai, I., Szalay, A. S., Koo, D. C., Kron, R. G., & Munn, J. A. 1995, AJ, 110, 2655
Connolly, A. J., Szalay, A. S., Dickinson, M., SubbaRao, M. U., & Brunner, R. J. 1997, ApJ, 486, L11
Dahlén, T., & Fransson, C. 1999, A&A, 350, 349
Dressler, A., Smail, I., Poggianti, B. M., Butcher, H., Couch, W. J., Ellis, R. S., & Oemler, A. 1999, ApJS, 122, 51
Fernándes-Soto, A., Lanzetta, K. M., & Yahil, A. 1999, ApJ, 513, 34
Fontana, A., D'Odorico, S., Poli, F., Giallongo, E., Arnouts, S., Cristiani, S., Moorwood, A., & Saracco, P. 2000, AJ, 120, 2206
Goliath, M., Amanullah, R., Astier, P., Goobar, A., & Pain, R. 2001, A&A, 380, 6
Goobar, A., & Perlmutter, S. 1995, ApJ, 450, 14
Gwyn, S. 1995, M.S. thesis, Univ. Victoria
He, P., Zou, Z.-L., & Zhang, Y.-Z. 2000, Ap&SS, 274, 557
Kinney, A. L., Calzetti, D., Bohlin, R. C., McQuade, K., Storchi-Bergmann, T., & Schmitt, H. R. 1996, ApJ, 467, 38
Lilly, S. J., Tresse, L., Hammer, F., Crampton, D., & Le Fèvre, O. 1995, ApJ, 455, 108
Madau, P., Della Valle, M., & Panagia, N. 1998, MNRAS, 297, L17
Madau, P., Pozzetti, L., & Dickinson, M. 1998, ApJ, 498, 106
Metcalfe, N., Shanks, T., Fong, R., & Jones, L. R. 1991, MNRAS, 249, 498
Mobasher, B., Rowan-Robinson, M., Georgakakis, A., & Eaton, N. 1996, MNRAS, 282, L7
Nugent, P., Kim, A., & Perlmutter, S. 2002, PASP, submitted
Perlmutter, S., et al. 1999, ApJ, 517, 565

Poggianti, B. M., Smail, I., Dressler, A., Couch, W. J., Berger, A. J., Butcher, H., Ellis, R. S., & Oemler, A. 1999, ApJ, 518, 576
Puschell, J. J., Owen, F. N., & Laing, R. A. 1982, ApJ, 275, 57
Riess, A. G., et al. 1998, AJ, 116, 1009
Riess, A. G., et al. 2001, ApJ, 560, 49
Sawicki, M. J., Lin, H., & Yee, H. K. C. 1997, AJ, 113, 1
Schechter, P. 1976, ApJ, 203, 297
Wang, L., Höflich, P., & Wheeler, J. C. 1997, ApJ, 483, L29
Wang, Y., Bahcall, N., & Turner, E. L. 1998, AJ, 116, 2081